Sustainable Chemical Engineering
https://ojs.wiserpub.com/index.php/SCE/

UNIVERSAL WISER PUBLISHER

Research Article

Effect of Annealing on Structural, Optical, and Magnetic Properties of $Zn_{0.90}Ni_{0.10}P_2$ Nanoparticles

Nakka Praveenkumar[1], Nasina Madhusudhana Rao[2], Mathew K. Moodley[1*]

[1]Discipline of Physics, University of KwaZulu-Natal, Westville Campus, Private Bag X54001, Durban, 4000, South Africa
[2]Department of Physics, School of Advanced Sciences, VIT-AP University, Inavolu, Beside AP Secretariat, Amaravati, Andhra Pradesh, 522237, India
E-mail: moodleymk@ukzn.ac.za

Received: 15 October 2025; **Revised:** 24 November 2025; **Accepted:** 27 November 2025

Abstract: Zinc phosphide nanoparticles doped with Nickel ($Zn_{0.90}Ni_{0.10}P_2$) were created via a solid-state process and then vacuum-annealed at two distinct temperatures (573 K and 873 K) and pressures of 2×10^{-2} mbar. The impact of different annealing conditions on the synthetic materials' optical, magnetic, and structural properties was examined. The produced samples clearly maintained a tetragonal structure, as shown by the X-Ray Diffraction (XRD) analysis, and the diffraction peaks show no observable signs of extra nickel or other impurities. As the annealing temperature was raised from 573 K to 873 K, the crystallite size increased from 31.597 nm to 32.019 nm, and the lattice parameters showed a positive correlation from a = 8.1096Å, c = 11.1098Å to a = 8.1722Å, c = 11.1286Å. According to the Energy-Dispersive X-ray Spectroscopy (EDS) analysis, the dopant concentration closely resembles the intended atomic ratio. As the annealing temperature was raised, the $Zn_{0.90}Ni_{0.10}P_2$ nanoparticles' optical band gap increased from 1.443 eV to 1.449 eV. The analysis of the Vibrating Sample Magnetometer (VSM) data shows that the annealing temperatures and saturation magnetization are positively correlated. The values of saturation magnetization, coercivity, and retentivity at 573 K and 873 K $Zn_{0.90}Ni_{0.10}P_2$ are 0.1499 emu/g, 69.52 Oe, 0.0039 emu/g,0.1676 emu/g, 65.46 Oe, and 0.0040 emu/g, respectively.

Keywords: vacuum annealing, $Zn_{0.90}Ni_{0.10}P_2$ nanoparticles, ferromagnetism, optical band gap

1. Introduction

Spintronics has shown a specific benefit from the use of Diluted Magnetic Semiconductors (DMS). Electrons' inherent spin property, which has sparked much research in both the theoretical and practical realms, is the basis of spintronics technology.[1] The features and possible applications of each DMS material in magneto-optical and magneto-transport systems are distinct.[2] An alloy made up of both magnetic and nonmagnetic components is referred to as a dilute magnetic semiconductor, while a magnetic semiconductor is defined as the ordered arrangement of magnetic elements. Increased speed, data storage in small places, increased resistance, and lower power consumption are just a few benefits of DMS materials. These compounds are characterized by their low Curie temperatures and restricted semiconducting characteristics. The growth of spintronic applications has been greatly aided by the finding of ferromagnetism in transition elements-doped IV-VI,[3] III-V,[4] and II-VI[5] dilute magnetic semiconductors. Zinc phosphide (Zn_3P_2), a semiconducting material belonging to class II-V, is the subject of this investigation. It is described as an

DOI: https://doi.org/10.37256/sce.7120268915

inexpensive, polar, mixed-valent, earth-abundant, and ecologically safe semiconductor. As seen by the wide coverage in scholarly literature, the scientific community has demonstrated a strong interest in researching zinc phosphide's properties in relation to the development of thin-film photovoltaic cells and its possible applications in solar energy research. The improvement of magnetic semiconductors and half-metallic ferromagnetism has been the subject of much study in recent years. It is clear from the prior literature review that little research has been done on the use of Zn_3P_2 material in combination with different dopants, including Ti-doped Zn_3P_2,[6] Fe-doped Zn_3P_2,[7] and Q-doped Zn_3P_2 with different elements (Q = V, Cr, Mn, Fe, Co).[8] Ab initio investigations came after these reviews. Ti-doped Cd_3P_2,[9] Mn-doped $ZnAs_2$,[10] Mn-doped Zn_3As_2,[11] and Mn-doped Zn_3As_2[12] are among the compounds from the same group that have been studied in the literature study. Sathyamurthy et al. researched the structural and optical characteristics in vacuum and spoke about the impact of annealing based on the annealing effect.[13,14] Electronic structure of the valence band in crystalline Zn_3P_2 as a function of annealing temperature was studied by synchrotron radiation photoemission.[15] Recently, we have studied the optical, magnetic, and structural properties of transition metals doped Zn_3P_2 nanoparticles using the solid-state reaction technique.[16-21] According to II-V diluted magnetic semiconductors, transition metals are doped into semiconductor Zn_3P_2 nanoparticles, carrier-induced ferromagnetism is produced more easily. It is imperative to synthesize the Zn_3P_2-based ferromagnetic material, whose physical and structural features must be clearly characterized, in order to comprehend the underlying mechanism in all of these operations. Experimental investigations verified and demonstrated that the synthesis techniques and ambient circumstances employed for sample synthesis have a significant impact on Ferromagnetism (FM).

Nickel is a crucial dopant to raise the Curie Temperature (Tc) above room temperature among all of these magnetic metals. Ni^{2+} is unique and one of the most effective dopant elements that improves optical, electrical, and magnetic properties because of its chemical stability when occupying Zn^{2+} sites.[22] In view of its appropriate ionic radius, electronic configuration, and magnetic nature, which make it extremely compatible with the Zn site in the host lattice, nickel (Ni) was selected as the dopant for Zn_3P_2. Since Ni^{2+} ionic radius (0.69 Å) is similar to Zn^{2+} (0.74 Å), substitutional insertion is possible without causing appreciable lattice deformation. Additionally, Ni has a partly filled $3d^8$ structure that might create localized magnetic moments and perhaps mediate ferromagnetic interactions through Bound Magnetic Polarons (BMPs) or carrier exchange processes like Ruderman-Kittel-Kasuya-Yosida (RKKY). At ambient temperature, diluted magnetic semiconductors with varying Ni content compositions were found to exhibit both paramagnetic and ferromagnetic properties by certain researchers.[23] The temperature stability of the doped metal ions, which determine the material's physical characteristics, is crucial for real-world applications since DMS include a proportion of transition elements.

The results of the literature review indicate that a number of experimental methods have been used to study the optical, magnetic, and structural properties of transition elements doped with zinc phosphide (Zn_3P_2). Vacuum annealing encourages atomic diffusion and grain growth, which enhances crystallinity and lowers structural defects. Sharper, more intense peaks in X-Ray Diffraction (XRD) patterns, suggesting better crystal order and potential Zn_3P_2 phase stabilisation. In addition to preventing contamination and oxidation, the vacuum environment preserves the Zn_3P_2 stoichiometry. Furthermore, little is known about how vacuum annealing at various temperatures affects the phase purity and magneto-optical correlations in Ni-doped Zn_3P_2 nanoparticles. In order to provide insights into adjustable functionality for optoelectronic and spintronic applications, this work attempts to clearly correlate annealing temperature, crystallite formation, band-gap modulation, and magnetic responses. This work is novel because (i) it produces Ni-doped Zn_3P_2 using an economical and energy-efficient solid-state synthesis route; (ii) it systematically investigates the effects of thermal treatment on a 10% Ni doping level, an area that is largely unexplored in the literature at the moment; and (iii) it shows that basic thermal processing can improve material performance without the need for additional chemical reagents, solvents, or high-energy equipment. This helps create more environmentally and financially friendly semiconductor production processes.

2. Experimental work

2.1 *Synthesis*

Figure 1 displays the Zn_3P_2 system's flow chart doped with Ni. Nickel-doped ($Zn_{0.90}Ni_{0.10}P_2$) zinc phosphide

nanoparticles were synthesized via the standard solid-state reaction method. Nickel phosphide (Ni_2P) and zinc phosphide (Zn_3P_2) are two chemical substances acquired from Sigma Aldrich. First, the mortar and pestle were scrubbed with acetone to begin cleaning. It took around 16 hours to crush the zinc phosphide and nickel phosphide compounds thoroughly. Upon completion of the grinding process for the pure materials, it was found that the dopant ions tended to form a homogeneous and uniform distribution by clustering together in close proximity. A programmable microcontroller was used to regulate the furnace in which the powder samples were kept after being moved into a small quartz tube. Pellets were formed from the powder samples and sintered in a vacuum at 1,073 K. After that, the sintered pellets were ground into fine powder. In order to progressively bring the synthesized nanoparticles to room temperature, they were annealed in a vacuum (2×10^{-2} mbar) at 573 K and 873 K and maintained there for 5 hours. The proper reaction time was maintained with a 5 °C/min to 10 °C/min heating/cooling rate. To ensure reproducibility, the synthesis was repeated three times independently, and all measurements were performed on each batch. The results were consistent within experimental uncertainty, confirming the reliability of the observed structural, optical, and magnetic properties.

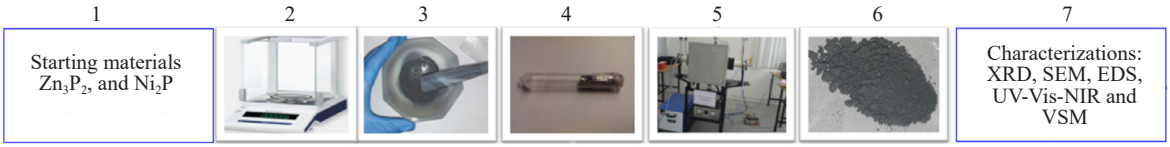

Figure 1. Flow chart of $Zn_{0.90}Ni_{0.10}P_2$ nanoparticles

2.2 *Characterizations techniques*

This study focused on a few examinations, including XRD using the Rigaku-mini flex-600 equipment. Cu Kα radiation, with a wavelength of 1.5406 Å, was used in XRD to determine the crystalline structure of the nanoparticles. The data were collected over a 2θ range of 20°-90°, with a step size of 0.02° and a scan rate of 1° min^{-1}. A Scanning Electron Microscope (SEM) (JSM-IT 500) running at an acceleration voltage of 10-15 kV was used to analyze the surface morphology. With an accelerating voltage of 15 kV and an acquisition time of roughly 60 s per spectrum, Energy-Dispersive X-ray Spectroscopy (EDS) attached to the SEM was used to confirm the elemental composition. A UV-Vis-NIR spectrophotometer (Perkin Lambda 365) was used to record the optical absorption spectra in the 200-1,100 nm wavelength range, with a spectral resolution of 1 nm. A Vibrating Sample Magnetometer (VSM) (Lakeshore 7410 S) was used to measure the magnetic properties at room temperature (300 K) with an applied magnetic field range of ± 15,000 Oe.

3. Results and discussions

3.1 *Structural properties*

The Zn_3P_2 system is shown in Figure 2a. The X-ray diffraction pattern was examined to analyze the peaks displayed in the 573 K and 873 K annealed samples, which demonstrated a distinct tetragonal structure of Zn_3P_2. The results obtained precisely match the Joint Committee on Powder Diffraction Standards (JCPDS) cards (Reference No. 74-1156). An analogous setup was described by Zawawi, I.K. EI.[24] With 137 atoms, Zn_3P_2 is a member of the P42/nmc space group. The lattice parameters of Zn_3P_2 are $a = b = 8.0970$ Å and $c = 11.4500$ Å, and its angles are $\alpha = \beta = \gamma = 90°$.[21]

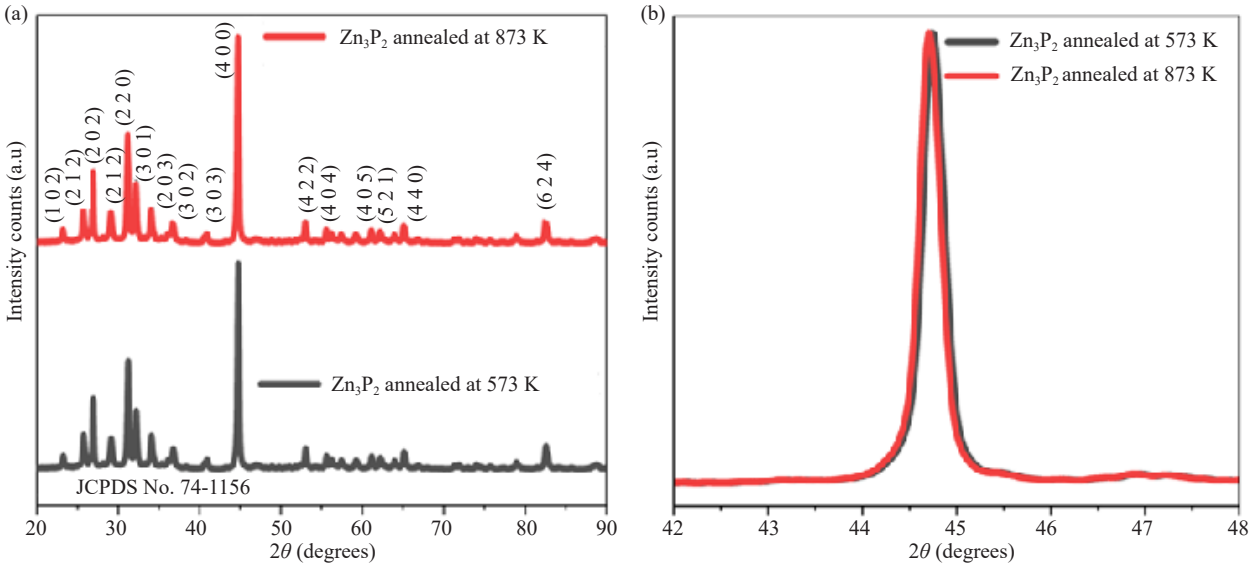

Figure 2. (a) XRD patterns of pure (573 K and 873 K) in the 2θ range of 20° to 90° and (b) plane (4 0 0), angle between 42°-48°

The high crystalline quality of Zn_3P_2 is shown by the sharp intensity and distinct patterns of the diffraction peaks of the pure system (at 573 K and 873 K). Figure 2b displays the Zn_3P_2 (473 K and 873 K) system's primary (4 0 0) diffraction peak in the 2θ range between 42.0° and 48°. The two annealed temperatures did not show any peak shifts.

In Figure 3a, $Zn_{0.90}Ni_{0.10}P_2$ nanoparticles at various annealing temperatures of 573 K and 873 K are shown. Figure 3a findings reveal that there are no additional peaks in the X-ray diffraction pattern that would suggest dopant ions (Ni) or other contaminants. This result confirms the tetragonal structure of Zn_3P_2, suggesting that the nickel dopants in the Zn_3P_2 material have been effectively substituted.

In Figure 3b, the (4 0 0) 2θ angle (42°-48°) is represented by the $Zn_{0.90}Ni_{0.10}P_2$ composition and the annealed temperatures. Possible explanations for the observed variations in the 2θ value include the effects of temperature and Ni concentration. Zn^{+2} (0.74 Å) and Ni^{+2} (0.69 Å) have different ionic radii, causes the lower side of the 2θ peak to shift toward smaller angles. Using several formulas, we examined structural characteristics such as crystallite size, microstrain, dislocation density, and lattice parameters that are described below.

$$\text{Crystallite size } D = \frac{K\lambda}{\beta \cos\theta} \tag{1}$$

$$\text{micro-strain } \varepsilon = \frac{\beta \cos\theta}{4} \tag{2}$$

$$\text{Dislocation density } \delta = \frac{1}{D^2}, \tag{3}$$

and

$$\frac{1}{d^2} = \left(\frac{h^2 + k^2}{a^2} + \frac{l^2}{c^2} \right) \tag{4}$$

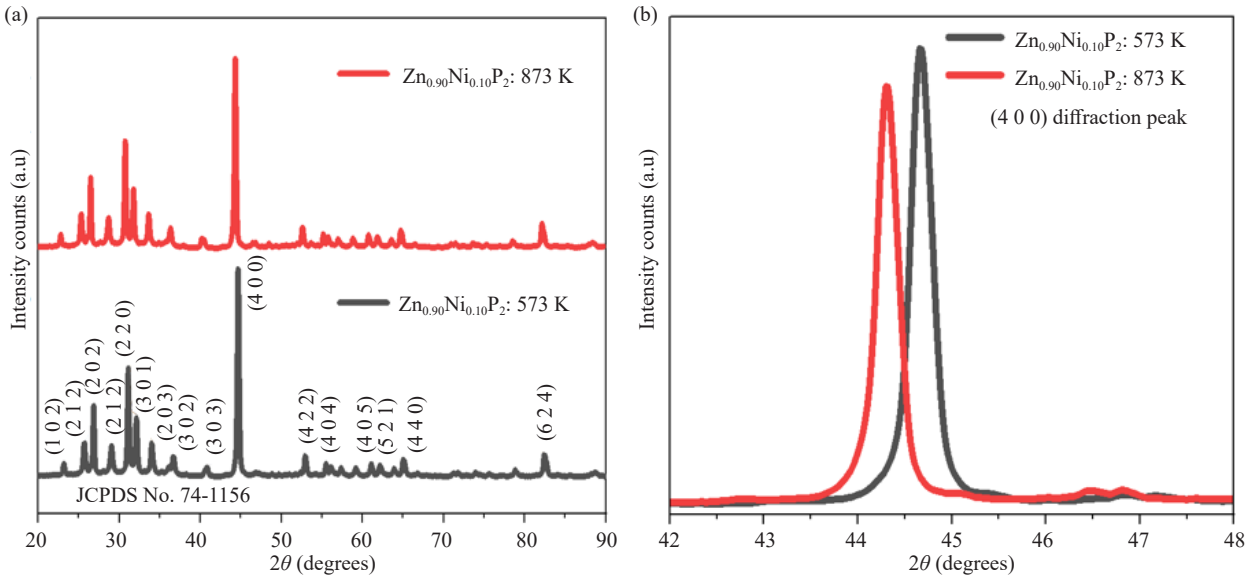

Figure 3. (a) XRD diffraction peak of $Zn_{0.90}Ni_{0.10}P_2$ (573 K and 873 K) nanoparticles in the 2θ range of 20° to 90° and (b) (4 0 0) predominate peak at 42° to 48°

Table 1. Structural parameters of Ni-doped Zn_3P_2 at 573 K and 873 K

System name	2θ (degree)	Crystallite size D (nm)	a (Å)	c (Å)	Microstrain ($\times 10^{-3}$)	Dislocation density ($\times 10^{15}$ m^{-2})
Zn_3P_2: 573 K	44.74	31.607 ± 0.45	8.0959 ± 0.004	11.0998 ± 0.005	1.097 ± 0.010	1.0010 ± 0.030
Zn_3P_2: 873 K	44.70	31.602 ± 0.42	8.1028 ± 0.004	11.1066 ± 0.005	1.097 ± 0.011	1.0012 ± 0.028
Ni:Zn_3P_2: 573 K	44.66	31.597 ± 0.40	8.1096 ± 0.004	11.1198 ± 0.005	1.094 ± 0.012	1.0015 ± 0.025
Ni: Zn_3P_2: 873 K	44.30	32.019 ± 0.38	8.1722 ± 0.005	11.1286 ± 0.006	1.083 ± 0.013	0.9753 ± 0.024

In this case, D stands for crystallite size, K for the constant, λ for wavelength, β for full-width half maximum, h, k, and l for miller indices, and a and c for lattice parameters. The XRD characteristics at 573 K and 873 K include crystallite size, microstrain, dislocation density, and lattice parameters, as shown in Table 1. The pure Zn_3P_2 and Ni-doped crystallite sizes are 31.607 nm, 31.602 nm, 31.596 nm, and 32.019 nm, respectively at 573 K and 873 K. No variation was observed in the crystallite size at 573 K and 873 K, at pure Zn_3P_2. Ni doped and temperature effect, the crystallite size was increased from 31.597 nm to 32.019 nm. At 573 K and 873 K, pure Zn_3P_2 and Ni-doped microstrain and dislocation density are 1.097, 1.097, 1.094, 1.083, 1.0010, 1.0012, 1.0015, and 0.9753, respectively. There was no difference in microstrain and dislocation density between 573 K and 873 K for the pure Zn_3P_2 system. The strain (1.094 to 1.083) and dislocation density decreased (1.0015 to 0.9753), due to the effect of Ni and temperature. The influence of Ni and temperature caused the lattice parameter to rise from $a = b = 8.1096$ Å, $c = 11.1198$ Å to $a = b = 8.1722$ Å, $c = 11.1286$ Å. Variations in the ionic radius of Zn and Ni as well as the formation of internal stress inside the generated samples may be the cause of this occurrence. Therefore, the sample's crystalline character has been reinforced by the heat treatment. The lattice parameters shown in the films indicate that the dopants are activated after annealing, so the lattice parameter rises, and the additional element occupies the host matrix's interstitial site. According to Balaraju et al.,[25] similar results were discussed.

3.2 *Elemental studies*

As seen in Figure 4, the elemental composition of ($Zn_{0.90}Ni_{0.10}P_2$) nanoparticles at 573 K and 873 K was examined using EDS. Analysing the spectra of the Zn_3P_2: 573 K and 873 K samples doped with Ni revealed the presence of Zinc

(Zn), Phosphorus (P), and Nickel (Ni) in atomic ratios that almost matched the predicted values.

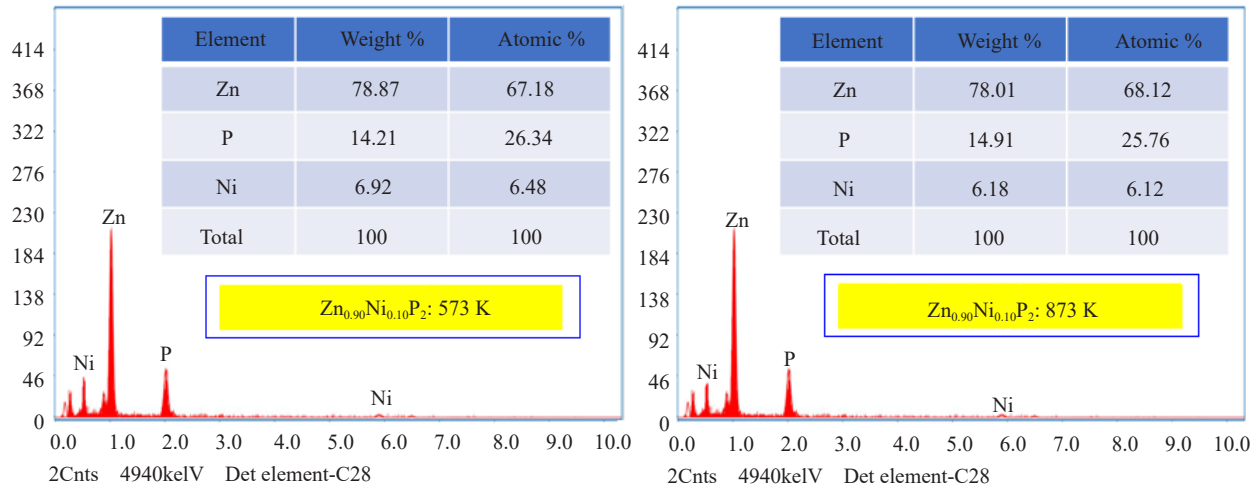

Figure 4. EDS spectra of $Zn_{0.90}Ni_{0.10}P_2$ nanoparticles, at 573 K and 873 K

3.3 *Surface morphological studies*

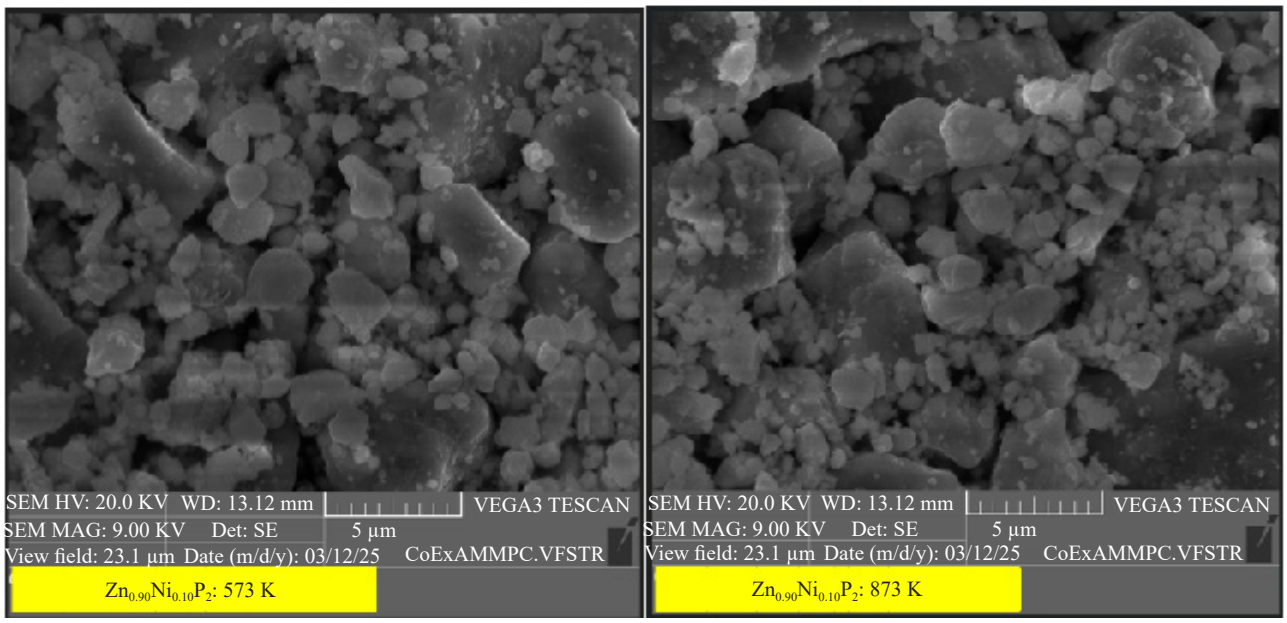

Figure 5. SEM pictures of $Zn_{0.90}Ni_{0.10}P_2$ nanoparticles

The SEM images of the Ni-doped Zn_3P_2 system at 573 K and 873 K are shown in Figure 5. The examination of Zn_3P_2 nanoparticles doped with nickel was the main focus of the study. As seen in Figure 5, the investigation included nickel concentrations, especially the $Zn_{0.90}Ni_{0.10}P_2$ sample. Higher doping concentrations and temperature in the pure system were shown to cause the production of spherical morphologies and the conversion of fine aggregates into larger aggregates, according to SEM images. In contrast to the results of the SEM analysis, which are shown in Table 1, the X-ray diffraction results show that the crystallite size is smaller. The degree of agglomeration depends on the

temperature and dopant concentration; as the dopant concentration rises, atoms inside the pure molecule are displaced.

3.4 *Optical properties*

Figure 6a shows the diffused reflectance spectra of undoped Zn_3P_2 nanoparticles at temperatures of 573 K and 873 K, covering a wavelength range of 200 nm to 1,100 nm. The pure nanoparticles exhibit a significant degree of Infrared (IR) reflection. Both 573 K and 873 K samples exhibit the same reflectance, as shown in Figure 6a. The following equation is used for calculation to find the Kubelka-Munk function, represented as F(R).

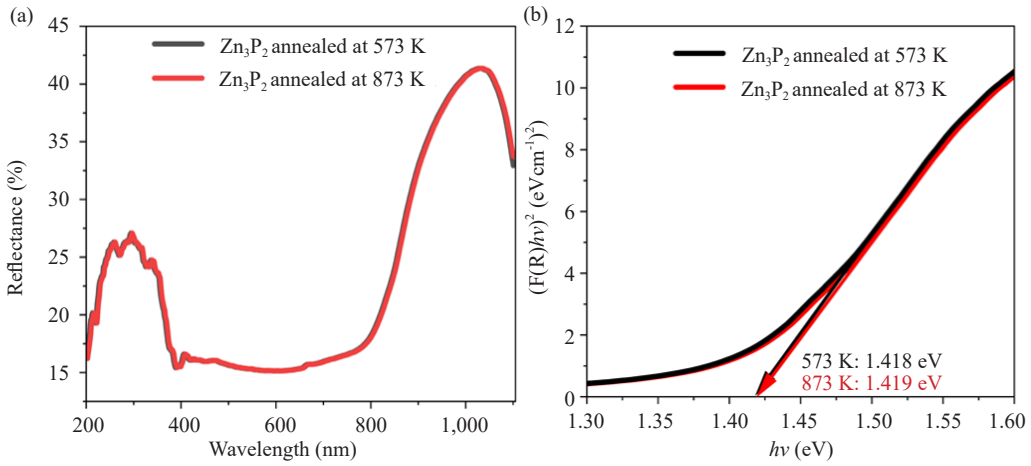

Figure 6. (a) Diffused reflectance spectra of pure nanoparticles at 573 K and 873 K and (b) plot of $(F(R)h\nu)^2$ versus hν of pure nanoparticles at 573 K and 873 K

$$F(R) = \frac{\alpha}{s} \tag{5}$$

$$\alpha h\nu = (F(R) \cdot s)h\nu = A\left(h\nu - E_g\right)^n$$

Where F(R) is the function of reflectance, absorption coefficient (α) and the scattering coefficient (s). Utilizing the Tauc equation, the optical band gap of all synthesized and pure samples was determined. Accordingly, the constants A and h stand for Planck's constant. In this case, E_g stands for the optical band gap, and $h\nu$ stands for a photon's energy. 1/2 is chosen as the value of 'n' in the case of direct authorized transitions. We may then expand the linear part of the absorption coefficient graph, which was shown as a function of the square of the product of photon energy ($h\nu$) and F(R), where α is equal to zero. The optical band gap of Zn_3P_2 at 573 K and 873 K is shown in Figure 6b. There is little change in the optical band gap at 573 K (1.418 eV) and 873 K (1.419) as the temperature increases.

Figure 7a shows the reflectance spectra of the Ni-doped Zn_3P_2 system in the wavelength range of 200 nm to 1,100 nm. The same reflectance was noted at 573 K and 873 K in the Ni-doped system. Figure 7b displays the optical band gap values of Ni-doped samples at 573 K and 873 K in the energy range of 1.30 eV to 1.60 eV. An optical band gap of 1.5 eV was observed in Zn_3P_2-only nanoparticles, according to a prior work.[14] The optical band gap rises with temperature from 1.443 eV to 1.449 eV. Due to the Burstein-Moss phenomenon, the optical band gap may increase as the Ni concentration increases. It takes more energy to go from the valence band to the conduction band because the Fermi level moves there and takes up some of the lowest levels. In comparison to the Ni-doped Zn_3P_2 nanoparticles without any heat treatment, the measured band gap is marginally greater (1.428 eV).[17] There are no documented cases of annealing effects on a virgin (Zn_3P_2) system.

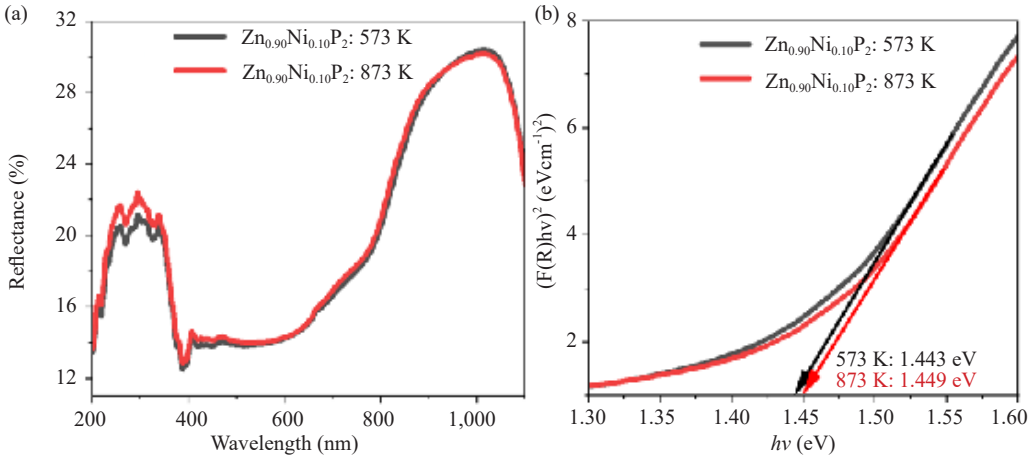

Figure 7. (a) DRS spectra of Ni-doped samples at 573 K and 873 K and (b) optical band gap

3.5 *Magnetic properties*

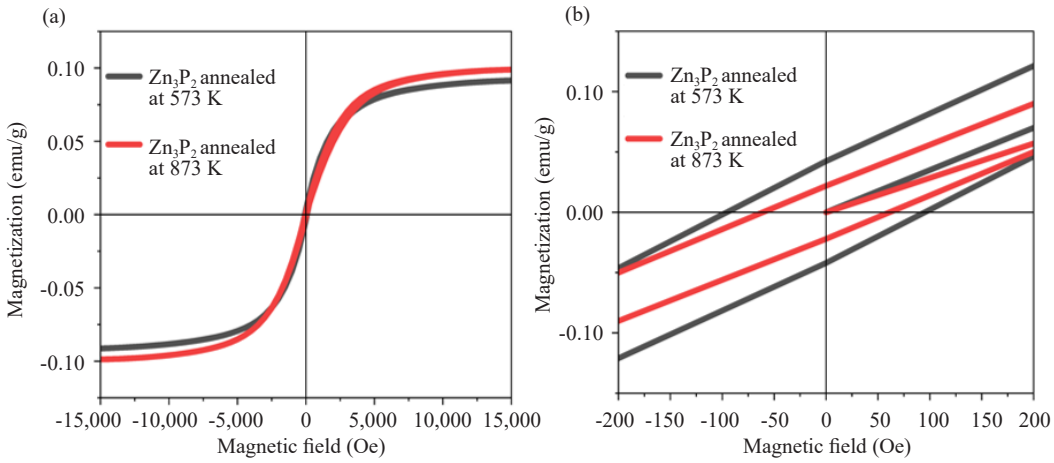

Figure 8. (a) M-H loop of Zn_3P_2 at 573 K and 873 K, field range of -15,000 Oe to + 15,000 Oe and (b) -200 Oe to + 200 Oe

The connection between magnetization (B) and applied field (H) for Zn_3P_2 nanoparticles at 573 K and 873 K is shown in Figure 8a. The hysteresis loop describes the magnetic field's range, which is -15,000 Oe to + 15,000 Oe. The Ferromagnetic (FM) material present in the diamagnetic lattice of the undoped Zn_3P_2 combination might be the cause of this phenomenon. V.S. Dang investigated the properties of Zn_3P_2 at room temperature in a 2007 research paper. Under these circumstances, Zn_3P_2 was shown to be stable and to have ferromagnetic characteristics.[26] At room temperature, the dopant ion Ni_2P displays ferromagnetic behavior.[29] Increasing the temperature to 573 K and 873 K caused the saturation magnetization to significantly rise from 0.0935 emu/g to 0.0963 emu/g. In the enlarged range of -200 Oe to + 200 Oe, Figure 8b displays the Zn_3P_2 nanoparticle at 573 K and 873 K. The saturation magnetisation (Ms), coercivity (Hc), and retentivity (Mr) of each sample were measured and are displayed in Table 2. According to Table 2, the coercivity and retentivity decreased from 97.94 Oe to 63.62 Oe when the temperature increased to 573 K and 873 K.

At 573 K and 873 K, the M-H curves of Ni-doped Zn_3P_2 nanoparticles are shown in Figure 9a. Regarding the impact of temperatures 573 K and 873 K on magnetic movement, the B-H hysteresis loop offers important information on the magnetic behaviour of the material. The saturation magnetization rose between 573 K and 873 K, from 0.1499 emu/g to 0.1676 emu/g. Both the dopant concentration and the ambient temperature affect the two previously stated parameters. The observed phenomenon is indicative of the magnetic exchange interaction resulting from variations in

the nickel concentration. For Zn_3P_2 nanoparticles doped with Ni, the magnetization versus the applied magnetic field (M-H) curve is shown in Figure 9b across the magnetic field range of -400 Oe to + 400 Oe.

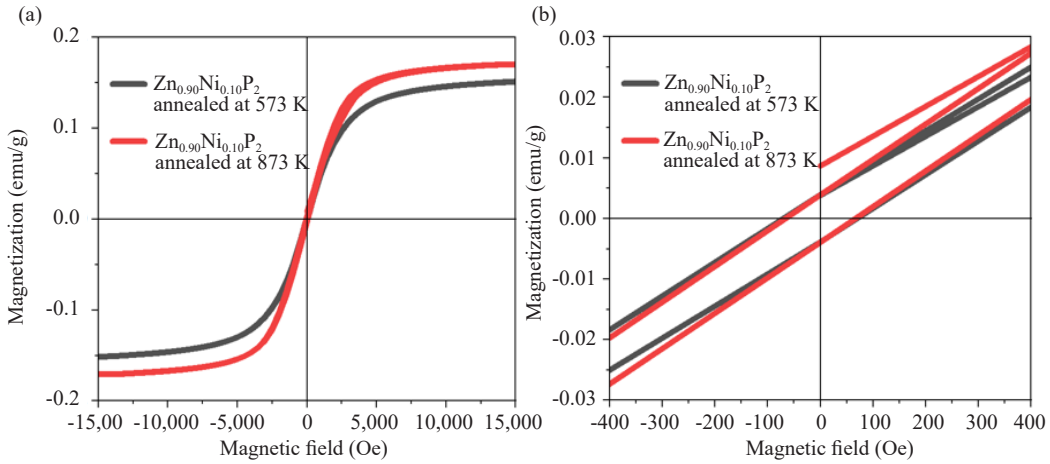

Figure 9. (a) M-H curve of Ni-doped nanoparticles at 573 K and 873 K, at -15,000 Oe to + 15,000 Oe and (b) -400 Oe to + 400 Oe

Table 2. Parameters of M-H curve

System name	Magnetization (M_s) (emu/g)	Coercivity (Hc) (Oe)	Retentivity (Mr) (emu/g)
Zn_3P_2: 573K	0.0935	97.94	0.0044
Zn_3P_2: 873K	0.0963	63.62	0.0024
Ni: Zn_3P_2: 573K	0.1499	69.52	0.0039
Ni: Zn_3P_2: 873K	0.1676	65.46	0.0040

According to Table 2, when the temperature was raised to 573 K and 873 K, the coercivity dropped (69.52 Oe → 65.46 Oe) and the retentivity rose from 0.0039 emu/g to 0.0040 emu/g. The transition elements doped in Zn_3P_2 were not compared using the hysteresis loop approach. Instead, several researchers used density functional theory-based ab initio experiments to study these elements' magnetic properties. To study the magnetic characteristics of transition elements (V, Cr, Mn, Fe, and Co) doped with Zn_3P_2, G. Jaiganesh et al. conducted ab initio investigations.[6,8] The ferromagnetic phase of a Ti-doped Zn_3P_2 matrix was identified by ab initio research. According to Jaiganesh et al., doped cation (Fe) d-like electrons are the primary source of magnetism.[7] Significant Fermi-level behaviour and spin-splitting are seen in the doped cation d-like state. While the doped cation's d-electrons play a major role in the compound's total magnetic moment (4.00 μB per unit cell), the Zn and P components also make minimal contributions. The transition elements Ni (2.80-3.50 μB) has been observed to have an effective magnetic moment experimentally.[28] According to Kai Zeppenfeld et al., Ni_2P compounds behave like paramagnets between 2 K and 300 K.[29]

There are various probable causes for the room temperature ferromagnetism seen in the produced samples. The initial possibility is the formation of secondary phases; however, this is readily refuted because XRD reveals no secondary phase peaks (Figure 3a). Second, diffraction peaks can be utilised to represent metals (in this example, nickel). Even though temperature and Ni are the primary drivers of ferromagnetism, XRD analysis reveals that there are no metal diffraction peaks up to the dopant concentration of the $Zn_{0.90}Ni_{0.10}P_2$ sample. The RKKY interaction between the conductive electrons of Zn_3P_2 and the spin-polarized electrons of Ni^{2+} ions is the third factor responsible for the ferromagnetic behaviour of Ni-doped Zn_3P_2 nanoparticles. These interactions may have their source in the spin polarisation of conductive electrons in the host lattice of Zn_3P_2. Furthermore, after a long-range exchange contact, Ni's local spin-polarized electrons show the same spin direction as conductive electrons. The material acquires ferromagnetic

characteristics because of this exchange interaction. A similar explanation for the existence of ferromagnetism was presented by Robina Ashraf et al.[30]

The experimental study literature review of the Zn_3P_2 system doped with transition metals is shown in Table 3. The observed magnetization in this research, however, is higher than that of previously published papers and to the one we previously reported without annealing.[16-21] The results of the study suggest that the observed outcomes be potentially beneficial for spintronic applications.

Table 3. Summary of Magnetic saturation (M_s) reported for different transition metal doped Zn_3P_2 nanoparticles

Sample	Magnetization (M_s) (emu/g)	References
$Zn_{0.94}Fe_{0.06}P_2$	0.1514	16
$Zn_{0.95}Ni_{0.05}P_2$	0.0388	17
$Zn_{0.94}Mn_{0.06}P_2$	0.1181	18
$Zn_{0.95}Ni_{0.02}Mn_{0.03}P_2$	0.0521	19
$Zn_{0.96}Fe_{0.02}Ni_{0.02}P_2$	0.0936	20
$Zn_{0.96}Mn_{0.02}Fe_{0.04}P_2$	0.0936	21
$Zn_{0.90}Ni_{0.10}P_2$ (873 K)	0.1676	Present study

4. Conclusion

In this work, a standard solid-state reaction method was used to create $Zn_{0.90}Ni_{0.10}P_2$ nanoparticles. The results of tests show that the amounts of nickel dopants are precisely integrated into the pure system. Additionally, there are no extra peaks in the synthesized samples, indicating that no contaminants present. All of the synthesized nanoparticles exhibit a tetragonal shape. According to the elemental analysis, the present EDS spectra closely resemble the intended atomic ratio (Ni). Particles in the realm of morphological studies tend to agglomerate. At 573 K and 873 K, the dopant concentration and temperature cause the optical band gap to increased from 1.443 eV to 1.449 eV. The vibrating sample magnetometer confirmed that the presence of dopant concentration and temperatures might cause a change from moderate ferromagnetism to ferromagnetism. At 573 K and 873 K, the saturation magnetization increased from 0.1499 emu/g to 0.1676 emu/g.

Acknowledgment

We appreciate the VSM facilities provided by IIT Madras.

Author contribution

The writing, characterization, and synthesis were completed by NPK. The results were discussed and the text was commented on by NPK, NMR and MKM.

Funding

No funding, money, or other assistance was obtained in the writing of this text, the author affirms.

Data availability

Upon reasonable request, data will be made accessible. This study's supporting data may be obtained from the corresponding author upon reasonable request.

Ethical approval

There is no research conducted by any of the authors using humans or animals in this article. There were no human or animal samples taken for this experiment.

Conflict of interest

The authors declare that he has no competing interests.

References

[1] Chen, W.; Buyanova, I. *Handbook of Spintronic Semiconductors*; CRC Press: State of Ohio, 2019.

[2] Žutić, I.; Fabian, J.; Sarma, S. D. O. Spintronics: Fundamentals and applications. *Rev. Mod. Phys*. **2004,** *76*(2), 323.

[3] Fukuma, Y.; Goto, K.; Senba, S.; Miyawaki, S.; Asada, H.; Koyanagi, T.; Sato, H. IV-VI diluted magnetic semiconductor Ge1-xMnxTe epilayer grown by molecular beam epitaxy. *J. Appl. Phys*. **2008,** *103*(5), 053904.

[4] Ohno, H.; Munekata, H.; Penney, Y. T.; Von Molnar, S.; Chang, L. L. Magnetotransport properties of p-type (In, Mn) As diluted magnetic III-V semiconductors. *Phys. Rev. Lett*. **1992,** *68*, 2664.

[5] Haury, A.; Wasiela, A.; Arnoult, T. A.; Cibert, J.; Tatarenko, S.; Dietl, T.; Aubigne, Y. M. Observation of a ferromagnetic transition induced by two-dimensional hole gas in modulation-doped CdMnTe quantum wells. *Phys. Rev. Lett*. **1997,** *79*, 511.

[6] Sekaran, J. G.; Mathi Jaya, S. Effect of partial Ti substitution at Zn sites on the Structural, Electronic and Magnetic Properties of Zn_3P_2. *Recent Trends Chem. Mater. Sci*. **2020,** *3*, 31-37.

[7] Jaiganesh, G.; Mathi Jaya, S. Half-metallic ferromagnetism in Fe-doped Zn_3P_2 from first-principles calculations. *AIP Conf. Proc*. **2014,** *1591*, 1081-1083.

[8] Jaiganesh, G.; Mathi Jaya, S. Magnetism, electronic structure and half-metallic property of transition metal (V, Cr, Mn, Fe, Co) substituted Zn_3P_2 dilute magnetic semiconductors: An ab-initio study. *Comput. Mater Sci*. **2015,** *102*, 85-94.

[9] Jaiganesh, G.; Mathi Jaya, S. Electronic structure and magnetism of titanium substituted Cd_3P_2: An ab-initio study. *AIP Conf. Proc.* **2018,** *1953*, 120062.

[10] Laiho, R.; Lisunov, K. G.; Lähderanta, E.; Zakhvalinskii, V. S. Magnetic properties of the new diluted magnetic semiconductor: evidence of MnAs clusters. *J. Phys. Condens. Matter*. **1999,** *11*, 555.

[11] Laiho, R.; Lisunov, K. G.; Lahderanta, E.; Zakhvalinskii, V. S. Magnetic MnAs nanoclusters in the diluted magnetic semiconductor $(Zn_{1-x}Mn_x)_3As_2$. *J. Phys. Condens. Matter*. **1999,** *11*, 8697.

[12] Denissen, C. J. M.; Nishihara, H.; Van Gool, J. C.; De Jonge, W. J. M. Magnetic behavior of the semimagnetic semiconductor $(Cd_{1-x}Mn_x)_3As_2$. *Phys. Rev. B*. **1986,** *33*, 7637.

[13] Sathyamoorthy, R.; Sharmila, C.; Natarajan, K.; Velumani, S. Influence of annealing on structural and optical properties of Zn_3P_2 thin films. *Mater. Charact.* **2007,** *58*, 745-749.

[14] Murali, K. R.; Gopalam, B. S. V. Effect of vacuum annealing on the electrical properties of Zn_3P_2 thin films. *J Mater Sci Lett.* **1998,** *7*, 125-129.

[15] Nelson, A. J.; Kazmerski, L. L.; Engelhardt, M.; Hochst, H. Valence-band electronic structure of Zn_3P_2 as a function of annealing as studied by synchrotron radiation photoemission. *J. Appl. Phys*. **1990,** *67*, 1393-1396.

[16] Praveenkumar, N.; Rao, N. M. Room temperature ferromagnetism in undoped and Fe doped Zn_3P_2 nanoparticles: Structural, optical and magnetic properties. *Solid State Sci*. **2024,** *151*, 107519.

[17] Praveenkumar, N.; Rao, N. M. Ni doped Zn_3P_2 nanoparticles: synthesis, structural, optical, and magnetic properties. *J. Supercond Nov. Magn*. **2024,** *37*(1), 165-177.

[18] Praveenkumar, N.; Rao, N. M.; Chakravarthi, M. K. Structural, optical, and magnetic properties of Mn doped Zn_3P_2 diluted magnetic semiconductor nanoparticles. *ECS J. Solid State Sci. Technol*. **2024,** *13*(5), 054003.
[19] Praveenkumar, N.; Rao, N. M. Transition metal (Ni, Mn) codoped Zn_3P_2 nanoparticles: effect on structural, optical and magnetic properties. *Nano Express* **2023,** *4*(4), 045009.
[20] Praveenkumar, N.; Madhusudhana Rao, N. The effect of Fe and Ni dual-doping on the structural, optical and magnetic properties of Zn_3P_2 nanoparticles. *Applied Physics A* **2024,** *130*(5), 271.
[21] Praveenkumar, N.; Madhusudhana Rao, N. Synthesis of (Mn, Fe) co-doped Zn_3P_2 nanoparticles: structural, optical and magnetic properties via solid-state reaction route. *J. Mater. Sci. Mater Electron*. **2024,** *35*(10), 719.
[22] Raja, K.; Ramesh, P. S.; Geetha, D. Synthesis, structural and optical properties of ZnO and Ni-doped ZnO hexagonal nanorods by Co-precipitation method. *SAA* **2014,** *120*, 19-24.
[23] Fabbiyola, S.; Sailaja, V.; Kennedy, L. J.; Bououdina, M.; Vijaya, J. J. Optical and magnetic properties of Ni-doped ZnO nanoparticles. *Alloy. Compd*. **2017,** *694*, 522-531.
[24] El Zawawi, I. K.; Moez, A. A.; Hammad, T. R.; Ibrahim, R. S. Phase transformation and disorder effect on optical and electrical properties of Zn_3P_2 thin films. *SAA* **2012,** *94*, 378-383.
[25] Balaraju, B.; Kaleemulla, S. Effect of annealing on structural, optical and magnetic properties of $Ce_{0.95}Fe_{0.05}O_2$ nanoparticles. *Vacuum* **2019,** *167*, 10-15.
[26] Yoo, Y. G. Ferromagnetism-to-paramagnetism transition in the ZnMnO system. *J. Korean Phys. Soc.* **2008,** *52*, 1398-1401.
[27] Zhang, D.; Zhou, X.; Liu, J.; Dong, L.; Zhao, J.; Xie, Y.; Sun, W. Selective synthesis of $Ni_{12}P_5$ and Ni_2P nanoparticles: Electronic structures, magnetic and optical properties. *MSEB* **2021,** *273*, 115389.
[28] Ferenc, W.; Osypiuk, D.; Sarzyński, J.; Głuchowska, H. Complexes of Mn (II), Co (II), Ni (II), Cu (II) and Zn (II) with ligand formed by condensation reaction of isatin with glutamic acid. *Eclet. Quím.* **2020,** *45*(3), 12-27.
[29] Zeppenfeld, K.; Jeitschko, W. Magnetic behaviour of Ni3P Ni2P, NiP3 and the series $Ln_2Ni_{12}P_7$ (Ln = Pr, Nd, Sm, Gd Lu). *J Phys. Chem. Solids* **1993,** *54*(11), 1527-1531.
[30] Ashraf, R.; Riaz, S.; Bashir, M.; Khan, U.; Naseem, S. Structural and magnetic properties of Mn/Fe co-doped ZnO thin films prepared by sol-gel technique. *IEEE Transactions on Magnetics* **2014,** *50*(8), 1-4.